First-principles calculation of coincidence Doppler broadening of positron annihilation radiation

Z. Tang,[1] M. Hasegawa,[1,2] Y. Nagai,[2] M. Saito,[3] and Y. Kawazoe[1]
[1]*Institute for Materials Research, Tohoku University, Sendai 980-8577, Japan*
[2]*The Oarai Branch, Institute for Materials Research, Tohoku University, Oarai, Ibaraki 311-1313, Japan*
[3]*NEC Informatec Systems, Ltd., 34, Miyukigaoka, Tsukuba 305-8501, Japan*
(Received 24 July 2001; published 3 January 2002)

We report a first-principles method for calculating the momentum density of positron-electron pairs in materials, which can be accurately measured, in a wide momentum range, by means of coincidence Doppler broadening (CDB) of positron annihilation radiation. The calculation is based on the two-component density-functional theory within the local-density approximation. The electron and positron wave functions are calculated by means of the full-potential linearized-augmented-plane-wave method with use of semicore orbitals and of the pure plane-wave method, respectively. This hybrid basis set accurately determines the wave functions of core and valence electrons and is free from any shape or symmetry assumption for the positron wave function. The method is applied to two typical systems. i.e., Al and graphite having isotropic and anisotropic positron densities, respectively. The calculations agree well with experiments over the entire measurable momentum region. Especially, the calculations well reproduce the anisotropic high-momentum CDB tails of graphite, which originate from the quasi-two-dimensionally distributed positron. This reproduction suggests that the present method is applicable for a variety of materials.

DOI: 10.1103/PhysRevB.65.045108 PACS number(s): 78.70.Bj, 71.15.Dx, 71.60.+z

I. INTRODUCTION

A positron injected into solid is annihilated with a surrounding electron into two γ photons. The total momentum of the annihilated positron-electron pair is mainly owing to the electron since the positron is rapidly thermalized before annihilation.[1] The usual one-detector Doppler-broadening (DB) technique measures the Doppler shift in the energy of one of these two γ photons given rise by the longitudinal momentum component of the positron-electron pair along the photon emission direction. The technique thus profiles one-dimensional (1D) momentum-density distribution of the positron-electron pair along a chosen axis. Unfortunately, being hampered by high background, the one-detector DB technique can reliably measure only the positron annihilations with the valence electrons and with the low-momentum core electrons.

The coincidence DB technique registers the energies of both annihilation γ photons by using a couple of detectors in coincidence. The coincidence measurement much improves the peak-to-background ratio of the usual one-detector DB by three orders (as high as 10^5:1) and thus enables the profiling of the 1D momentum-density distribution of the positron-electron pair over wide momentum region.[2–4] The CDB technique has great application potential for the studies of the electronic and atomic structures of defects in solids, since it is possible to identify the elements around the positron annihilation sites based on the characteristic shapes of the CDB spectra at the high-momentum region. This technique has been extensively employed in the recent positron annihilation studies[4–12] and has met with impressive success in identifying the impurity atoms bound to the vacancies in semiconductors[5,6] and in exploring and characterizing nanosize precipitates in dilute alloys.[7,8]

The experimental success have stimulated intensive theoretical studies for the CDB spectra in materials.[13–17] A computational scheme,[13] in which the electrons and positron are described by free atomic orbitals and model-fitted functions, respectively, is found to be successful in interpreting the experiments. Recently, a first-principles scheme based on the Korringa-Kohn-Rostoker (KKR) band-structure method was reported;[17] the calculation for Al crystal has demonstrated that, by treating the semicore electrons ($2s^2 2p^6$) of the Al atoms as the band electrons (namely, in the same manner as that for the valence electrons) to take account of the crystalline environment effects, the calculated CDB agrees with the experiment quantitatively. Now it is clear that, to achieve good agreement between theory and experiment over wide momentum region it is necessary to describe well the positron wave function, *all* the electron wave functions, and the positron-electron correlation effect over the *entire* system under study, i.e., from the low-momentum interstitial regions to the high-momentum core regions. However, the schemes proposed so far assumed the positron wave functions being spherically symmetric around the nuclei in calculating the positron-core-electron annihilations,[13,17] which significantly limits their application to the systems with this assumption being violated. One of the important examples is the defects in solids where the density of the trapped positron is rather anisotropic around the nuclei neighboring the defects.

In this paper we present a first-principles scheme for the CDB calculation with widely applicable potential. In our approach, the electron wave functions are calculated by using the full-potential linearized-augmented-plane-wave (FLAPW) method. The positron wave function, which has no node and no rapid oscillation around the nuclei, is expanded as the plane waves without any shape or symmetry assumption. The positron-electron correlation effect is calculated based on state-of-the-art two-component density-functional (TCDF) theory within the local-density approximation (LDA),[18–20] which has been shown by the recent experimental and theoretical works[17,21–23] to be very reliable in repro-

ducing positron annihilation characteristics for a variety of systems, such as the bulk materials and the defects. The method is employed to calculate the CDB spectra for the Al and graphite crystals. The latter is a typical layer-structure material where the anisotropic positron-density distribution is expected. The calculations are compared with the experiments and good agreement is observed over the entire experimental momentum region. Especially, the calculations are found to well reproduce the anisotropic high-momentum tails of the CDB spectra for graphite, demonstrating clearly the ability of the present method for various systems.

II. METHOD

In this section, we present the method to calculate the momentum-density distribution of the positron-electron pair in perfect crystals. In the Appendix, we explain how to extend the method for the defect studies.

A. Outline

We first outline how the momentum-density distribution of the positron-electron pair is calculated within the LDA based on the TCDF theory. We consider the system where a single positron is perfectly delocalized in the infinite crystal, so that the electronic states are not perturbed by the positron whose concentration is zero. Then, we begin with the conventional electron band-structure calculation. The Bloch electron wave function $\psi_{i\mathbf{k}}(\mathbf{r})$, where i and $\mathbf{k}$ are the band index and crystal momentum, respectively, is given by the Kohn-Sham equation based on the LDA (in atomic units) as

$$\{-\tfrac{1}{2}\nabla^2+V_H(\mathbf{r})-V_{\mathrm{nuc}}(\mathbf{r})+\mu_{e\text{-}e}[n(\mathbf{r})]\}\psi_{i\mathbf{k}}(\mathbf{r})=\epsilon_{i\mathbf{k}}\psi_{i\mathbf{k}}(\mathbf{r}), \tag{1}$$

where n is the charge density constructed from the wave functions, $-V_{\mathrm{nuc}}$ is the nuclear attractive potential, and V_H is the Hartree potential, $\int(n(\mathbf{r}')/|\mathbf{r}-\mathbf{r}'|)d\mathbf{r}'$. The exchange-correlation potential $\mu_{e\text{-}e}$ is deduced from numerical results for the homogeneous electron gas having the density n.[24] The above equation is solved by means of the self-consistent method.

In the next step, we calculate the positron wave function $\psi_+(\mathbf{r})$, which is given by

$$\{-\tfrac{1}{2}\nabla^2-V_H(\mathbf{r})+V_{\mathrm{nuc}}(\mathbf{r})+\mu_{e\text{-}p}[n(\mathbf{r})]\}\psi_+(\mathbf{r})=\epsilon_+\psi_+(\mathbf{r}), \tag{2}$$

where $\mu_{e\text{-}p}$ is the positron-electron correlation potential, which is deduced from the numerical results for the system of a single positron in the homogeneous electron gas having the density n. Since the annihilated positron is in the ground state, the positron wave function is at the Γ point.

After the electron and positron wave functions are determined, the momentum density of the positron-electron pair at the momentum $\mathbf{p}$ is given by[25,26]

$$\rho(\mathbf{p})=\sum_{i,\mathbf{k}} f(\epsilon_{i\mathbf{k}})|A_{i\mathbf{k}}(\mathbf{p})|^2 \tag{3}$$

where $f(\epsilon_{i\mathbf{k}})=2\,\theta(E_F-\epsilon_{i\mathbf{k}})$ is the occupation number and $A_{i\mathbf{k}}(\mathbf{p})$ is the momentum wave function of the positron-electron pair

$$A_{i\mathbf{k}}(\mathbf{p})=\frac{1}{N}\int_{N\Omega} e^{-i\mathbf{pr}}\psi_{i\mathbf{k}}(\mathbf{r})\,\psi_+^{\mathrm{enh}}(\mathbf{r})\,d\mathbf{r}. \tag{4}$$

In the above expression, $\psi_+^{\mathrm{enh}}(\mathbf{r})$ is the enhanced positron wave function defined as $\psi_+^{\mathrm{enh}}(\mathbf{r})=\psi_+(\mathbf{r})\sqrt{g(\mathbf{r})}$ with $g(\mathbf{r})$ being the enhancement factor and $N\Omega$ is the volume of the system containing N unit cells. As well as the positron-electron correlation potential $\mu_{e\text{-}p}$, the enhancement factor g, which originates from the screening by electrons around the positron, is deduced from the results calculated for the system of single positron in homogeneous electron gas.

Here, we briefly explain the functional forms of $\mu_{e\text{-}p}$ and g. The correlation energy for the system consisting of a single positron in the homogeneous gas was calculated by Arponen and Pajanne (AP) who performed many-particle random-phase-approximation (RPA) calculations.[27] The numerical results obtained by AP are first parameterized by Boroński and Nieminen,[18] and later reparametrized by Puska, Seitsonen, and Nieminen (PSN).[19] As for the enhancement factor, PSN parameterized the numerical results obtained by Lantto, who performed a hypernetted chain calculation.[28] This PSN scheme has been shown by the recent experiment and theory to be very reliable in reproducing positron annihilation characteristics for a variety of systems. Therefore, we adopt this scheme in the present study.

B. Electron wave functions

In order to accurately describe the core electrons as well as the valence electrons, we adopt the FLAPW method to solve the electron Kohn-Sham equation (1). In this method, the valence-electron wave function $\psi_{i\mathbf{k}}(\mathbf{r})$ in Eq. (1) is expanded by the LAPW basis set $\{\varphi_{\mathbf{K}}(\mathbf{r})\}$,

$$\psi_{i\mathbf{k}}(\mathbf{r})=\sum_{\mathbf{K}_n} C_{i\mathbf{k}}(\mathbf{K}_n)\,\varphi_{\mathbf{K}_n}(\mathbf{r}), \tag{5}$$

where $|\mathbf{K}_n|=|\mathbf{k}+\mathbf{G}_n|$ has the maximum value, K_{cut}, and $\mathbf{G}_n$ is the reciprocal lattice vector. The LAPW basis function $\varphi_{\mathbf{K}}(\mathbf{r})$ is defined as[29,30]

$$\varphi_{\mathbf{K}}(\mathbf{r})=\Omega^{-1/2}e^{i\mathbf{Kr}} \tag{6}$$

for $\mathbf{r}$ in the interstitial region, and

$$\varphi_{\mathbf{K}}(\mathbf{r})=e^{i\mathbf{K}(\mathbf{R}_I+\mathbf{R}_\alpha)}\sum_{lm} i^l[A_{lm}^{\alpha}(\mathbf{K})u_{\alpha l}(E_l,r_0) + B_{lm}^{\alpha}(\mathbf{K})\dot{u}_{\alpha l}(E_l,r_0)]Y_{lm}(\hat{r}_0) \tag{7}$$

for $\mathbf{r}$ inside the muffin-tin (MT) spheres. In the above equation, $\mathbf{r}_0=\mathbf{r}-\mathbf{R}_I-\mathbf{R}_\alpha$, where $\mathbf{R}_I$ is the unit-cell position and $\mathbf{R}_\alpha$ is the position of the αth atom measured from the position at $\mathbf{R}_I$. $u_{\alpha l}(E_l,r_0)$ and $\dot{u}_{\alpha l}(E_l,r_0)$, respectively, are the radial wave function with the energy parameter E_l, and its energy derivative in the MT sphere. All other symbols have their usual meaning.[29–31] The radial wave function and its

energy derivative are matched to the value and the derivative of the plane wave ($e^{i\mathbf{Kr}}$) on the MT sphere boundary by the coefficients $A_{lm}^{\alpha}(\mathbf{K})$ and $B_{lm}^{\alpha}(\mathbf{K})$.

As well as the wave functions, the potential, and the charge density are expanded into the plane-wave representation in the interstitial regions as[32–34]

$$\begin{pmatrix} V(\mathbf{r}) \\ n(\mathbf{r}) \end{pmatrix} = \sum_{\mathbf{G}} \begin{pmatrix} V(\mathbf{G}) \\ n(\mathbf{G}) \end{pmatrix} e^{i\mathbf{Gr}}, \tag{8}$$

and into the spherical harmonic representation in the MT spheres as

$$\begin{pmatrix} V(\mathbf{r}) \\ n(\mathbf{r}) \end{pmatrix} = \sum_{lm} \begin{pmatrix} V_{lm}(r_0) \\ n_{lm}(r_0) \end{pmatrix} Y_{lm}(\hat{r}_0). \tag{9}$$

As for the core electrons, there are high lying and relatively extended core electrons in the atoms (for instance, the $2s$ and $2p$ states in the Al atoms). These core electrons play important role in the CDB experiments; they actually dominate the shapes of the CDB profiles at the middle momentum region. As shown by the recent first-principles study,[17] the free atomic orbitals are insufficient to describe such core states, thus more accurate *ab initio* crystal wave functions are needed to calculate their momentum-density distributions. In the present approach, the extended core states are considered as the semicore states[35,36] and are calculated in the same manner as the valence states to take account of the off-site overlaps of the wave functions. For those low-lying core states, the atomic wave functions are employed, which are calculated self-consistently using the scalar-relativistic version of the Schrödinger equation having the spherically averaged crystal potential.

C. Positron wave function

In this subsection, we solve the single-particle equation of the positron Eq. (2), by use of the plane-wave basis set, i.e.,

$$\psi_{+}(\mathbf{r}) = \Omega^{-1/2} \sum_{|\mathbf{G}|<G_{+}^{\max}} C_{+}(\mathbf{G}) \epsilon^{i\mathbf{Gr}}. \tag{10}$$

The accuracy of this basis set is determined by the cut-off wave vector, $G_{+}^{\max}$ and as mentioned in the following section, it is larger than the cut-off wave vector $G_{-}^{\max}$, for the electron calculations in the interstitial region. By use of this basis set, the positron single-particle equation (2) is converted into the following secular equation

$$\sum_{\mathbf{G}'} [\tfrac{1}{2}|\mathbf{G}'|^2 \delta_{\mathbf{G}'-\mathbf{G}} + V_{+}^{\mathrm{eff}}(\mathbf{G}-\mathbf{G}')] C_{+}(\mathbf{G}') = \epsilon_{+} C_{+}(\mathbf{G}), \tag{11}$$

where the positron effective potential $V_{+}^{\mathrm{eff}}(\mathbf{G})$ in the G space is the summation of the Coulomb potential of the nuclei $[V_{\mathrm{nuc}}(\mathbf{G})]$, of the Hartree potential of the electron charge $[-V_H(\mathbf{G})]$, and of the positron-electron correlation potential for the positron. This potential is expanded in the region $|\mathbf{G}|<2G_{+}^{\max}$ and how to construct the potential is explained later. The secular equation of the positron wave function (11) is solved by using the iteration minimization technique[37] initiated by Car and Parrinello[38] and the positron energy and wave function of the ground state are then obtained.

In order to construct the above-mentioned effective potential $V_{+}^{\mathrm{eff}}(\mathbf{G})$, we first deduce the electron density $n(\mathbf{G})$ in the G space from the results of the FLAPW calculation. The charge densities of valence and semicore electrons in the regions of interstitial part and in the MT spheres, respectively, are given by

$$\begin{aligned} n^{\mathrm{INT}}(\mathbf{G}) = {} & n(\mathbf{G})\,\theta(G_{-}^{\max}-|\mathbf{G}|) \\ & - \sum_{\alpha,\mathbf{G}'} e^{i(\mathbf{G}'-\mathbf{G})\mathbf{R}_{\alpha}} n(\mathbf{G}')\,\theta(G_{-}^{\max}-|\mathbf{G}|) \\ & \times \frac{3\Omega_{\mathrm{MT}_{\alpha}}}{\Omega} \frac{j_1(|\mathbf{G}'-\mathbf{G}|R_{\mathrm{MT}_{\alpha}})}{|\mathbf{G}'-\mathbf{G}|R_{\mathrm{MT}_{\alpha}}}, \end{aligned} \tag{12}$$

and by

$$\begin{aligned} n^{\mathrm{MT}}(\mathbf{G}) = {} & \frac{4\pi}{\Omega} \sum_{\alpha lm} e^{-i\mathbf{GR}_{\alpha}} i^{-l} Y_{lm}(\hat{G}) \\ & \times \int_0^{R_{\mathrm{MT}_{\alpha}}} r_0^2 n_{lm}(r_0) j_l(Gr_0)\, dr_0, \end{aligned} \tag{13}$$

where $\Omega_{\mathrm{MT}_{\alpha}}$ and $R_{\mathrm{MT}_{\alpha}}$ are the volume and the radius of the MT sphere α, respectively. The core-electron density is also obtained by use of an expression similar to Eq. (13) [since the charge distribution is spherical, only the $l=0$ term in Eq. (13) should be considered].

After the total electron density $n(\mathbf{G})$ is obtained as explained above, we evaluate the Hartree term as $-V_H(\mathbf{G}) = -4\pi n(\mathbf{G})/G^2$. In order to evaluate the electron-positron correlation potential, we first construct the electron charge density $n(\mathbf{r})$ at a real-space mesh by using Eqs. (8) and (9), then the positron-electron correlation potential is calculated in this real-space mesh, and finally this potential is transformed into the G space. The Coulomb potential of the nuclei is calculated as $V_{\mathrm{nuc}}(\mathbf{G}) = \Sigma_{\alpha} 4\pi Z_{\alpha} e^{-i\mathbf{GR}_{\alpha}}/G^2$ where Z_{α} is the number of the nuclear charges at the αth site. In this equation, the component $\mathbf{G}=0$ is omitted, since it is canceled exactly by the electron Hartree potential with $\mathbf{G}=0$.

D. Momentum density

In this subsection, we explain how to evaluate the momentum density of positron-electron pair that was given in Eqs. (3) and (4). For the valence and semicore electrons, the overlap integral in Eq. (4) contains two kinds of contributions, i.e., that from the interstitial region $[A_{i\mathbf{k}}^{\mathrm{INT}}(\mathbf{p})]$ and that from the MT spheres $[A_{i\mathbf{k}}^{\mathrm{MT}}(\mathbf{p})]$. The interstitial contribution $A_{i\mathbf{k}}^{\mathrm{INT}}$ can be obtained by first integrating the plane-wave overlap of the electron and positron over the entire system and then subtracting the integral at the MT spheres, namely,[39]

$$A_{i\mathbf{k}}^{\mathrm{INT}}(\mathbf{p})=\delta_{\mathbf{p}'-\mathbf{k}}\times\Bigg[P_{i\mathbf{k}}(\mathbf{G}')-\sum_{\alpha,G}e^{i(\mathbf{G}-\mathbf{G}')\mathbf{R}_\alpha}P_{i\mathbf{k}}(\mathbf{G})\times\frac{3\Omega_{\mathrm{MT}_\alpha}}{\Omega}\frac{j_1(|\mathbf{G}-\mathbf{G}'|R_{\mathrm{MT}_\alpha})}{|\mathbf{G}-\mathbf{G}'|R_{\mathrm{MT}}}\Bigg],\tag{14}$$

where $\mathbf{p}=\mathbf{p}'+\mathbf{G}'$ with $\mathbf{p}'$ being inside the first Brillouin zone (FBZ). $P_{i\mathbf{k}}(\mathbf{G})$ is the Fourier component of the overlap wave function of positron and electron in the interstitial region given by $P_{i\mathbf{k}}(\mathbf{G})=\Sigma_{\mathbf{K}_n}C_{i\mathbf{k}}(\mathbf{K}_n)C_+^{\mathrm{enh}}(\mathbf{G}-\mathbf{G}_n)$, where $\mathbf{G}_n=\mathbf{K}_n-\mathbf{k}$ and $C_+^{\mathrm{enh}}(\mathbf{G})$ is the Fourier component of $\psi_+^{\mathrm{enh}}(\mathbf{r})$.

For the contribution from the MT spheres, we obtain the following form

$$A_{i\mathbf{k}}^{\mathrm{MT}}(\mathbf{p})=\delta_{\mathbf{p}'-\mathbf{k}}\Omega^{-1/2}\sum_{\alpha lm}\sum_{\mathbf{K}_n,\mathbf{G}}C_{i\mathbf{k}}(\mathbf{K}_n)C_+^{\mathrm{enh}}(\mathbf{G})\times e^{i(\mathbf{G}_n+\mathbf{G}-\mathbf{G}')\mathbf{R}_\alpha}[A_{lm}^{\alpha}(\mathbf{K}_n)f_{lm}^{\alpha}(\mathbf{p}-\mathbf{G})+B_{lm}^{\alpha}(\mathbf{K}_n)h_{lm}^{\alpha}(\mathbf{p}-\mathbf{G})],\tag{15}$$

where f_{lm}^{α} and h_{lm}^{α} are the Fourier transforms of the augmented spherical function and of its energy derivative in the MT sphere α given by

$$\begin{pmatrix}f_{lm}^{\alpha}(\mathbf{k})\\ h_{lm}^{\alpha}(\mathbf{k})\end{pmatrix}=4\pi Y_{lm}(\hat{k})\int_0^{R_{\mathrm{MT}_\alpha}}r_0^2 j_l(kr_0)\begin{pmatrix}u_{\alpha l}(E_l,r_0)\\ \dot{u}_{\alpha l}(E_l,r_0)\end{pmatrix}dr_0.\tag{16}$$

The above formulas allow to calculate $A_{i\mathbf{k}}(\mathbf{p})=A_{i\mathbf{k}}^{\mathrm{INT}}(\mathbf{p})+A_{i\mathbf{k}}^{\mathrm{MT}}(\mathbf{p})$, and thus the momentum density is evaluated by use of Eq. (3).

As for the core electrons, the FLAPW calculation gives the localized orbitals at the MT spheres, $\phi_{nlm}^{\alpha}(\mathbf{r}_0)=R_{nl}^{\alpha}(r_0)Y_{lm}(\hat{r}_0)$, with the principal quantum number n. By assuming that the overlaps between localized orbitals are zero, we obtain the momentum density of the positron-core-electron pair as

$$\rho_{\mathrm{core}}(\mathbf{p})=\frac{2}{\Omega}\sum_{\alpha,nlm}\left|\sum_{\mathbf{G}}C_+^{\mathrm{enh}}(\mathbf{G})e^{i\mathbf{G}\mathbf{R}_\alpha}\chi_{nlm}^{\alpha}(\mathbf{p}-\mathbf{G})\right|^2,\tag{17}$$

where

$$\chi_{nlm}^{\alpha}(\mathbf{k})=4\pi i^{-l}Y_{lm}(\hat{k})\int_0^{\infty}r_0^2 j_l(kr_0)R_{nl}^{\alpha}(r_0)dr_0.\tag{18}$$

III. RESULTS AND DISCUSSION

In this section, the method described in the preceding section is employed to calculate the momentum-density distributions of the positron-electron pair in the crystals of aluminum and graphite. The calculations are compared with our experiments, which allows us to evaluate how well the present method reproduces the experiments over wide momentum region. Especially, the pronounced anisotropies at the high-momentum region are observed for graphite both experimentally and theoretically demonstrating the importance of the positron wave function around the core regions.

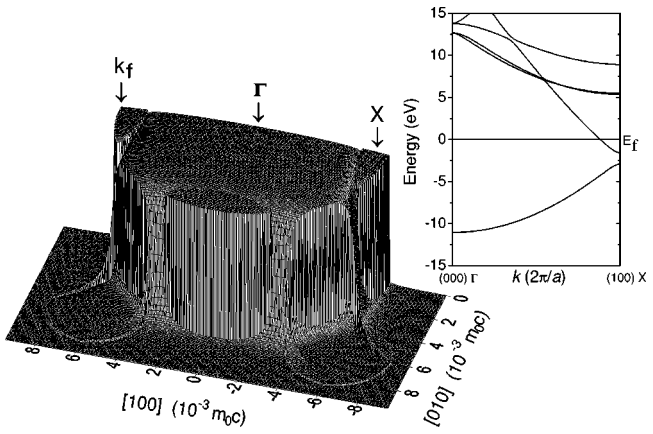

FIG. 1. Perspective plot of calculated momentum-density distribution of positron-valence-electron pair at the half [001] plane for Al (as for the momentum unit, 1.0 a.u.$=7.297\times10^{-3}m_0c$). The insert on the right shows the band structure along the [100] axis.

A. Aluminum

We start from the fcc aluminum since this system has been systematically studied by the positron annihilation technique in the past decades.[13,17,40] In the calculation, the experimental lattice parameter of $a=4.05$ Å (7.65 a.u.) is adopted. The contact-type MT sphere with the radius $R_{\mathrm{MT}}=2.70$ a.u. (which makes the nearest-neighboring MT spheres touching each other) is employed. The cutoff for the LAPW basis set is chosen as $K_{\mathrm{cut}}=4.0$ a.u. which yields a basis size of about 120 LAPW's per atom. The spherical harmonic expansion inside the MT spheres is up to $l_{\max}=8$. $G^{\max}$, the cutoff value of the wave vector used for depicting the electron charge density and potential in the interstitial regions, is set to $2K_{\mathrm{cut}}=8.0$ a.u. In the self-consistent calculation of the charge density, the Brillouin-zone integration is performed using the special k-points scheme developed by Chadi and Cohen.[41] A Monkhorst-Pack[42] type k mesh containing $25\times25\times25$ k points is sampled in the present work and the achieved self-consistency of the charge density (including the core electrons) is better than 0.01 me/(a.u.)^3. As mentioned in the preceding section, the $2s^22p^6$ core electrons of Al atom are treated as the semicore electrons. The crystal wave functions of these states are calculated in the same manner as the valence electrons by using different linearization energy windows.[36] For the positron, a large enough plane-wave basis set with the cutoff $G_+^{\max}=12.3$ a.u. is employed. It is noteworthy that further enlarging the plane-wave basis size does not increase much the computational effort for the positron wave function but does do so for the momentum-density distributions (in this work, the 3D momentum density $\rho(\mathbf{p})$ is calculated up to $p\sim80\times10^{-3}m_0c$). All the above parameters are carefully checked so that it is believed that the convergence has been achieved; for instance, the momentum densities along several highly symmetric lines calculated using $G_+^{\max}=14.8$ a.u. show no difference from the results presented in this paper.

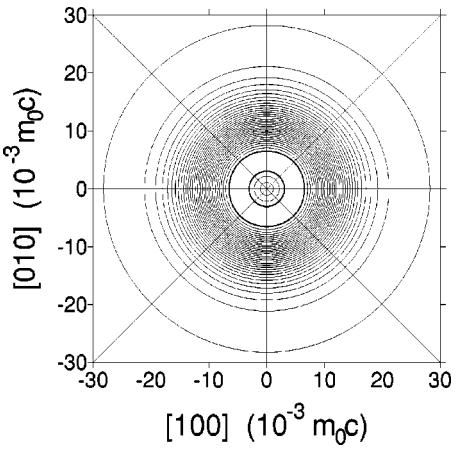

FIG. 2. Contour plot of calculated momentum-density distribution of positron-core-electron pair at the [001] plane for Al. The thick lines denote the maximum contour lines and the contour spacing is 3.0% of the maximum.

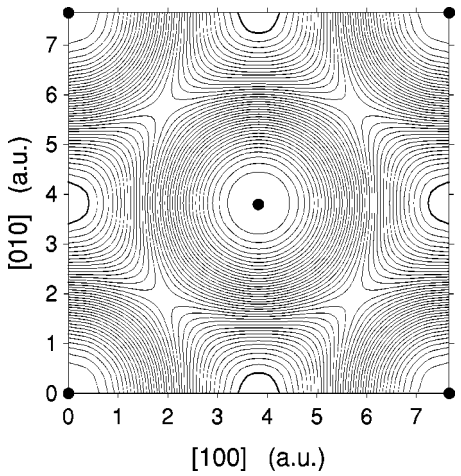

FIG. 3. Contour plot of calculated positron-density distribution at the [001] plane for Al. The thick lines denote the maximum contour lines and the contour spacing is 2.5% of the maximum. Solid circles denote the Al atoms.

Figure 1 shows the calculated momentum-density distribution of the positron-valence-electron pair at the half [001] plane for Al. Because of the nearly free-electron nature of Al, a very isotropic Fermi surface outline (i.e., the cross section of the Fermi surface with the [001] plane) is observed. However, the momentum-density distribution itself is anisotropic, which is manifested by the shoulderlike prominences around the X points at the BZ boundaries. The Al atom has three valence electrons ($3s^2 3p^1$), requiring two occupied bands in the FBZ. As shown in the insert of Fig. 1, the lower s band is fully filled up to the FBZ boundary, while the upper p band is half filled in the FBZ with the occupied momentum regions around the zone boundary. The shoulderlike prominences just present the momentum densities of the p-band electrons at the zone boundaries added to the continuous momentum-density background of the s-band electrons. A more interesting point in Fig. 1 is the momentum-density distribution out of the Fermi surface. Due to the selection rule of symmetry,[25] the Umklapp contributions of the s-band electrons become zero at some regions out of the FBZ. In such regions, only the shoulderlike momentum densities (Umklapp components) of the upper p band is visible so that the Fermi surface cutoff originated from the half filling of this band is still clear enough to be discriminated at these regions with relatively high momenta.

Figure 2 shows the calculated momentum-density distribution of the positron-core-electron pair for Al at the same [001] plane, where both the contributions from the semicore and core electrons are included. It is observed that the momentum-density distribution of the positron-core-electron pair is very isotropic. An important factor giving rise to this feature is the positron-density distribution. As shown in Fig. 3, the density distribution of the delocalized positron is rather isotropic in the core regions of the Al crystal, which leads to the fact that the positron equally samples the core electrons at different directions.

With the 3D momentum densities being calculated, it is ready to simulate the experimental CDB spectra. As mentioned in Sec. I, the CDB measures the longitudinal momentum densities of the positron-electron pair along the annihilation γ photon emission direction (p_z), which can be obtained in calculation by projecting the 3D momentum density $\rho(\mathbf{p})$ to this direction as

$$N(p_z) = \text{const} \times \int \rho(\mathbf{p}) dp_x dp_y . \tag{19}$$

In this work the CDB spectra along several directions are calculated and Fig. 4 presents the results along the crystallographic direction [001]. In addition, the partial contributions to the CDB spectrum from the positron annihilations with the valence electrons (summation of two conduction bands) and with the $2s$, $2p$ (summation of three semicore bands), and $1s$ core electrons are also presented in Fig. 4. From the par-

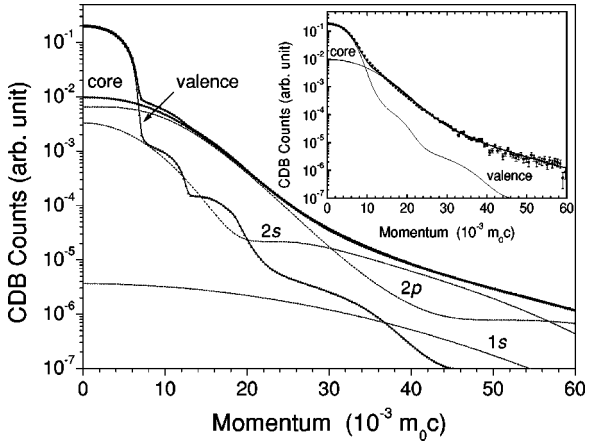

FIG. 4. Calculated coincidence Doppler broadening spectrum along the [001] direction for Al. Partial contributions of positron annihilations with valence and core electrons (which are further decomposed into the contributions of $1s$, $2s$, and $2p$ electrons) are also presented. The insert shows the comparison between experiment (solid circles with error bars) and theory (convoluted with the experimental resolution) (lines), and both the spectra are normalized to the same area.

tial contribution of the valence electrons in Fig. 4, we see clearly several steps due to the Fermi surface cutoff around 6.7, 13.0, and $20.0\times10^{-3}m_0c$. However, only the first two Fermi surface breaks can be discriminated from the total CDB spectrum, since when the momentum is increasing larger than the Fermi momentum, the CDB spectrum mainly represents the shape of the $2p$ electrons (up to $30\times10^{-3}m_0c$). Moreover, with further increasing the momentum, the contribution of the $2s$ electrons becomes the dominant component. Because the momentum-density distribution of the semicore and core electrons is very isotropic (Fig. 2), the calculated CDB spectra along several directions are found to be almost identical at the high-momentum region. This (together with Fig. 3) evidences that using the spherically symmetric positron wave function in the core regions is a good approximation for the Al crystal.

Next, we compare the theoretical results with the experiments. In our experiments, a single crystal Al sample was employed for the CDB measurements. The general description of the details of the experimental setup can be found in our previous works.[7] The inset of Fig. 4 compares the calculation [convoluted with the experimental resolution of 1.1 keV (about $4.3\times10^{-3}m_0c$)] with the experimental CDB spectrum along the [001] direction. The agreement between experiment and theory is found to be satisfactory over the entire momentum range. As reported by Mijnarends,[17] we also observe that when the atomic orbitals are employed for calculating the $2s^22p^6$ electrons instead of the semi-core-state wave functions, the agreement at high-momentum region becomes worse. This indicates that the crystal environment can modify the wave functions of the high-lying core electrons in the atoms, which may be detectable by using the positron CDB technique.

It is noticed that there are some slight discrepancies between experiment and theory around 10 and $18\times10^{-3}m_0c$ (Fig. 4). The calculation gives the momentum densities slightly lower (higher) than the experiments at the former (latter). The discrepancy around $18\times10^{-3}m_0c$ can be attributed to the overestimated enhancement for the $2p$ electrons in the present LDA scheme.[17] The discrepancy around $10\times10^{-3}m_0c$ may be relevant to a hot spot in the recent momentum-density studies.[43,44] It has been noticed in the recent high-resolution Compton scattering and positron two-dimensional angular correlation of annihilation radiation (2D-ACAR) experiments that the first-principles calculations tend to give lower valence-electron momentum densities at the tail region, above the Fermi momentum in metals (as that observed around $10\times10^{-3}m_0c$ in the inset of Fig. 4). One of possible reasons for such a discrepancy is the clear Fermi surface associated with the single-particle Kohn-Sham equation in the LDA picture, which gives rise to too sharp drop of the valence-electron momentum density above the Fermi momentum (Figs. 1 and 4). It has been shown that,[44] by considering the smearing of the Fermi surface due to the many-electron effect, the calculation for Al can be improved significantly. However, further investigating this issue beyond the LDA is out of the scope of the present paper.

Another possible source of the discrepancy is the LDA to the many-particle effect of the positron-electron correlation. Early theoretical studies[45,46] for the interacting positron-electron gases lead to a momentum-dependent enhancement factor, which increases significantly as the momentum approaches the Fermi surface but is strongly attenuated at the tail out of the Fermi surface. This enhancement factor results in a density prominence around Fermi surface and corrects efficiently the calculated momentum-density distributions for metals based on the free-electron-gas model. However, straightforwardly applying this enhancement factor to the present calculational results will enlarge the band-structure effect induced prominences around the X points (Fig. 1) and sharpen the discontinuity at the Fermi momentum, and thus may worsen the agreement between theory and experiment. The momentum-dependent enhancement factor was generalized to an energy-dependent form[47,48] and was further developed recently into a weighted-density-approximation (WDA) scheme.[49] As shown by Rubaszek, Szotec, and Tenmerman,[50] the WDA scheme can well reproduce the experimental results for Al.

Finally, we compare the calculated positron lifetime with the experiment. The positron lifetime (τ) is the inverse of the total annihilation rate (λ) of the positron-electron pair, which is given by

$$\lambda = \frac{\pi r_0^2 c}{8\pi^3}\int \rho(\mathbf{p})d\mathbf{p}. \tag{20}$$

Here r_0 denotes the classic electron radius. The present calculation gives the positron lifetime of 165 ps for the Al crystal, which is in good agreement with the experiment (163–166 ps) (Refs. 17, 51) and is also comparable with the values calculated by using other methods, such as the KKR (166 ps),[17] the linear muffin-tin orbital within the atomic-spheres approximation (LMTO-ASA) (165 ps),[52] etc.

B. Graphite

In the above subsection, we investigated a nearly isotropic momentum-density distribution of the positron-electron pair in Al. In this subsection, we turn to an anisotropic system, the crystal of graphite. As a prototypical layer structure material, the electronic structure of graphite exhibits pronounced anisotropies because of the presence of two distinct and completely different types of interatomic bonding. Previous studies[53–55] have revealed that the positron ACAR distributions (which mainly measure the momentum distributions of the positron-valence-electron pairs at the low-momentum region) in graphite are very anisotropic so that a marked bimodality with two peaks along the $p_{\|c}$ direction is observed. In this work, the present all-electron and full-potential method is employed to calculate the positron annihilation characteristics in graphite with careful attention paid to the momentum-density distributions at the high-momentum region. The calculations are compared with our previous pseudopotential calculations and recent CDB experiments.

In the calculations, the experimental lattice parameters[56] of $a=b=2.46$ Å (4.65 a.u.) and $c/a=2.72$ and the contact-type MT spheres with the radius $R_{\mathrm{MT}}=1.34$ a.u. are employed. The cutoff parameters are chosen as $K_{\mathrm{cut}}=5.5$ a.u.,

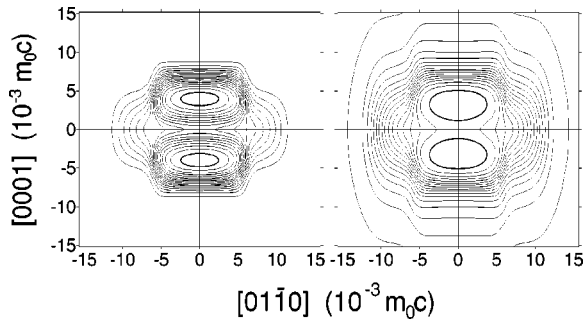

FIG. 5. Contour plots of calculated momentum-density distribution of positron-valence-electron pair (left panel) and ''pure'' valence-electron momentum-density distribution (right panel) at the $[2\bar{1}\bar{1}0]$ plane for graphite. The thick lines denote the maximum contour lines and the contour spacing is $\frac{1}{16}$ of the maximum.

$l_{\max}=8$, $G_{-}^{\max}=11.0$ a.u., and $G_{+}^{\max}=12.2$ a.u. A Monkhorst-Pack[42] type k mesh containing 1000 k points in the FBZ is sampled in this work and the 3D momentum density $\rho(\mathbf{p})$ is calculated up to $p\sim 80\times 10^{-3}m_0c$. Moreover, there is no semicore state in the carbon atom and its $1s^2$ electrons are calculated as the core electrons by using Eqs. (17) and (18).

Figure 5 shows the calculated momentum-density distribution of the positron-valence-electron pair at the $[2\bar{1}\bar{1}0]$ plane. Form this figure, it is observed that the momentum-density distribution of graphite is very anisotropic and the general shape of the distribution is dominated by the density variation along the [0001] direction. There is a bimodality observed along this direction with two pronounced peaks centered at $p_{[0001]}\sim\pm 4\times 10^{-3}m_0c$ on the [0001] axis. Moreover, along this direction the momentum density decreases rapidly when the momentum is increasing more than $8.5\times 10^{-3}m_0c$. On the contrary, the momentum density along the $[01\bar{1}0]$ direction decreases much slowly so that there are significant densities distributed around the $[01\bar{1}0]$ axis extending up to $p_{[01\bar{1}0]}\sim\pm 11.5\times 10^{-3}m_0c$, which results in two marked density prominences along this direction (Fig. 5).

The positron-density distribution plays an important role in producing the above-mentioned anisotropies. To demonstrate this, we plot the ''pure'' electron momentum-density distribution (EMDD) in Fig. 5, which is calculated by setting all the Fourier components of the enhanced positron wave function equal to zero except for $C_{+}^{\mathrm{enh}}(\mathbf{G}=0)=\Omega^{1/2}$. From the EMDD in Fig. 5, we find that, though the EMDD is anisotropic, its anisotropic features are much weaker compared with those of the momentum-density distribution of the positron-electron pairs. (For instance, only very small bimodal peaks are observed on the [0001] axis in the EMDD.) As shown in Fig. 6, the positron density is quasi-two-dimensionally distributed in graphite with its maxima between the layers. The positron significantly samples the low-momentum parts of the p_z orbitals of the carbon atoms in between the layers, and thus results in a much enhanced p character of the momentum-density distribution (manifested

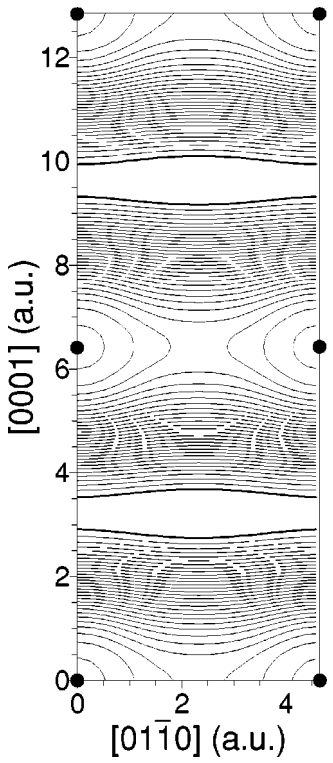

FIG. 6. Contour plot of calculated positron-density distribution at the $[2\bar{1}\bar{1}0]$ plane for graphite. The thick lines denote the maximum contour lines and the contour spacing is 3.3% of the maximum. Solid circles denote the carbon atoms.

by the pronounced bimodality) and in the rapid drop of the momentum density over $8.5\times 10^{-3}m_0c$ along the [0001] direction. While the positron sampling for the sp^2 hybrid orbitals in the layers is relatively homogenous so that the prominences of the momentum density along the $[01\bar{1}0]$ axis (originated from the positron annihilation with the sp^2 electrons) are close to the ''pure'' EMDD's at these regions (Fig. 5).

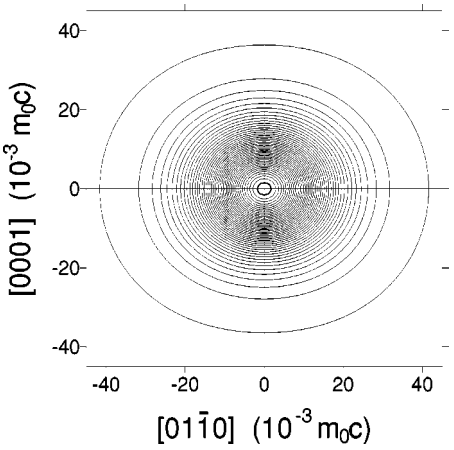

FIG. 7. Contour plot of calculated momentum-density distribution of positron annihilation with $1s$ core electrons at the $[2\bar{1}\bar{1}0]$ plane for graphite. The thick line denotes the maximum contour line and the contour spacing is 2.3% of the maximum.

Figure 7 shows the calculated momentum-density distribution of the positron annihilation with the $1s$ core electrons in graphite at the same $[2\overline{1}10]$ plane and this density distribution is also found to be anisotropic. As mentioned in the preceding paragraphs, the $1s$ core electrons are calculated by using Eqs. (17) and (18). The ''pure'' EMDD of the core states obtained by setting only $C_+^{\mathrm{enh}}(\mathbf{G}=0)=\Omega^{1/2}$ in Eqs. (17) and (18) is isotropic, namely,

$$\rho_{\mathrm{core}}^{\mathrm{EMD}}(\mathbf{p})=8\pi\sum_{\alpha,nl}(2l+1)\left|\int_0^\infty r_0^2 j_l(pr_0)R_{nl}^{\alpha}(r_0)dr_0\right|^2. \tag{21}$$

Thus, the observed anisotropies in the positron-core-electron annihilation entirely come from the positron sampling effect. As shown in Fig. 6, the positron-density distributions around the core regions are indeed anisotropic. The positron densities along the [0001] direction decrease rapidly to being vanishingly small at the nuclear sites so that the high-momentum components of $1s$ orbitals are suppressed along this direction (which is similar to the observed suppressing of the valence-electron momentum density above $p_{[0001]}\sim 8.5\times 10^{-3}m_0c$). As a result, the momentum-density distribution of the positron-core-electron pair becomes anisotropic with the lower densities along the [0001] direction.

We have compared the present calculations with our previous works[54,55] where the pseudopotential plane-wave scheme was adopted to calculate the valence-electron wave functions and the frozen-core orbitals of the free atoms were employed to describe the core electrons.[21] It is found that the pseudopotential scheme gives nearly the same results at the low-momentum region ($p<20\times 10^{-3}m_0c$), although at the high-momentum region the pseudopotential scheme does not give physically meaningful results because of the usage of the pseudo-wave-functions in the core regions. Furthermore, the calculated positron lifetime for the graphite bulk using the pseudopotential method (209.1 ps) agrees very well with the present calculation (210.0 ps). The good agreement between both the schemes indicates that, as long as concerning the positron ACAR distribution and lifetime, the pseudo-valence-wave-functions and frozen-atomic-core orbitals can well reproduce the experiments.[57]

Next, we project the calculated 3D momentum-density distribution $\rho(p)$ into the CDB spectra and compare them with the experiments. Since a highly oriented pyrolytic graphite (HOPG) sample (in which the c axes of the graphite crystals are oriented to the [0001] direction while the a and b axes are randomly oriented at the perpendicular plane) is employed in our experiments, only two kinds of CDB spectra, $N(p_{\|c})$ and $N(p_{\perp c})$, are typical. In the calculation, the former can be obtained straightforwardly by the 2D integrations for $\rho(\mathbf{p})$ at the perpendicular planes to the [0001] axis. To calculate the latter, angular averaging (before projection) for $\rho(\mathbf{p})$ at the perpendicular planes (to simulate the randomly oriented a and b axes) is necessary, namely,

$$N(p_{\perp c})=\mathrm{const}\times\frac{1}{2\pi}\int\rho(\sqrt{p_{\perp c}^2+p^2}\cos\varphi,$$

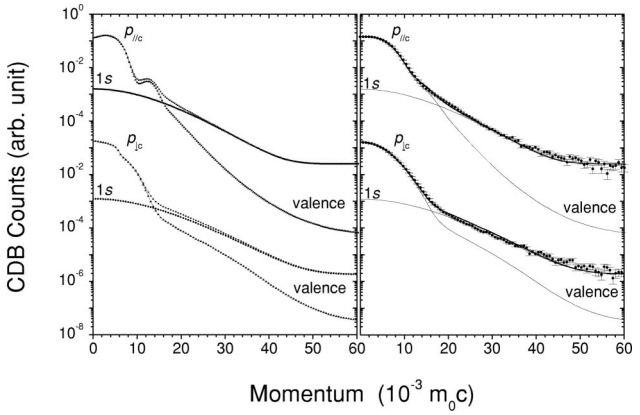

FIG. 8. Calculated coincidence Doppler broadening spectra and their partial contributions of valence and core ($1s$) electrons along the $p_{\|c}$ and $p_{\perp c}$ directions for highly oriented pyrolytic graphite (left panel). The right panel shows the comparisons between experiment (solid circles with error bars) and theory (convoluted with the experimental resolution) (lines), and for comparison the experimental and calculational spectra are normalized to the same area.

$$\sqrt{p_{\perp c}^2+p^2}\sin\varphi,p_{[0001]})d\varphi dp dp_{[0001]}. \tag{22}$$

Figure 8 presents the calculated CDB spectra for the HOPG. It is found that the 1D CDB spectra represent well the characteristic anisotropies observed in the 3D momentum-density distributions. For instance, there are a bimodality peak around $\sim 3\times 10^{-3}m_0c$ and a rapid momentum-density drop above $8\times 10^{-3}m_0c$ along the $p_{\|c}$ direction and a density prominence from ~ 6 to $12\times 10^{-3}m_0c$ and slightly higher momentum densities at the high-momentum region from ~ 20 to $45\times 10^{-3}m_0c$ along the $p_{\perp c}$ direction.

To verify the calculated anisotropic features, we carefully measured the CDB spectra along the $p_{\|c}$ and $p_{\perp c}$ directions for the HOPG sample (ZYA grade, Union Carbide Co.). The experiments are compared with the calculations [convoluted with the experimental resolution of 1.2 keV (about $4.7\times 10^{-3}m_0c$)] in Fig. 8 and good agreement is observed over the entire measurable momentum region. However, because of the smearing effect of the resolution, the anisotropic features of the experimental CDB spectra are less emphasized. Thus, we extract the CDB ratio of $N(p_{\perp c})/N(p_{\|c})$ (Fig. 9), which can highlight the anisotropic characteristics of the experimental CDB spectra.[4] As shown in Fig. 9, it is found that even for the ratio spectrum the agreement between experiment and theory is rather satisfactory. We clearly observe in both the experiments and calculations a ratio valley around $6\times 10^{-3}m_0c$ due to the bimodal peak of $N(p_{\|c})$, a ratio peak from 9 to $14\times 10^{-3}m_0c$ due to the rapid drop (prominence) of $N(p_{\|c})$ [$N(p_{\perp c})$] at this momentum region, and a continuous increase of the ratio from 20 to $40\times 10^{-3}m_0c$ due to the anisotropic positron sampling for the $1s$ core electrons. These observations, in particular, the observed high-momentum behaviors, manifestly demonstrate the importance of the positron wave functions around the core regions in the CDB studies.

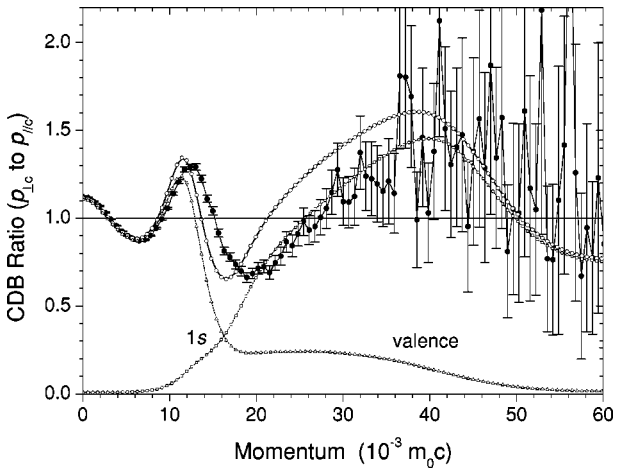

FIG. 9. Experimental (solid circles with error bars) and calculational (open circles) ratio curves of coincidence Doppler broadening spectrum along the $p_{\perp c}$ direction $[N(p_{\perp c})]$ relative to that along the $p_{\|c}$ direction $[N(p_{\|c})]$. Dashed lines denote the calculational partial contributions of valence and core $(1s)$ electrons to $N(p_{\perp c})$ relative to the total $N(p_{\|c})$. For comparison, before extracting ratio both the calculated $N(p_{\perp c})$ and $N(p_{\|c})$ or the partial contributions are convoluted with the experimental resolution.

IV. CONCLUSION

Based on the full-potential linearized-augmented-plane-wave (plane-wave) expansion for the electron (positron) wave functions and on the two-component density-functional theory within the local-density approximation, a first-principles scheme to calculate the positron annihilation characteristics in solids is reported. The highlight of the present method is the calculation (without any shape or symmetry assumption) for the wave functions of the positron-electron pairs at the core regions around the nuclei. As a result, the method can compute the momentum-density distribution of the positron-electron pair over wide momentum region, from the low-momentum interstitial region to the high-momentum core region, and is particularly suitable to study the coincidence Doppler broadening (CDB) of positron annihilation radiation in solids in which the one-dimensional projection of the momentum-density distribution of the positron-electron pair can be measured up to the high-momentum region. To verify the validity of the method, two typical systems, Al and graphite having isotropic and anisotropic positron-density distributions around the nuclei, respectively, are investigated experimentally and theoretically in this work. The calculated CDB spectra are found to agree well with the experiments over the entire measurable momentum region. Especially, for graphite the calculations well reproduce the anisotropic momentum-density distributions at the high-momentum region originated from the anisotropic positron sampling for the $1s$ core electrons of the carbon atoms. These successful results demonstrate clearly the importance of the positron wave function in the CDB studies and indicate that the present method can be applied to the CDB studies for a variety of systems, especially those with the anisotropic positron densities around the nuclei, such as the defects in solids.

ACKNOWLEDGMENTS

The authors would like to express their sincere thanks to Dr. T. Chiba of National Institute for Materials Science, Japan and Dr. Q. Sun for fruitful discussion, and to the Information Science Group of the Institute for Materials Research, Tohoku University, for its continuous support of using the Hitachi SR8000 supercomputing system. This work was partly supported by Grant-in-Aid for Scientific Research of the Ministry of Education, Culture, Sports, and Science and Technology (Grant Nos. 10450222, 12358005, 12640334, and 13305044).

APPENDIX

We here briefly explain how to extend the present method for the defect studies. To simulate the positron annihilation at the defect in solid, we employ a supercell containing the defect and a single positron. Within this approximation, the calculation for the defect is essentially the same as the one presented in Sec. II, except for the point that the perturbation of the trapped positron to the local electronic structure of the defect has to be taken into account and consequently, the self-consistency between the positron and electron densities is needed. To achieve this, two additional potential terms given rise by the localized positron, namely, the Hartree potential of positron density and the positron-electron correlation potential for the electrons, are needed to be added to the electron effective potential (1). Moreover, in order to employ the FLAPW method, these two additional potentials must be represented into the plane-wave representation in the interstitial region (8) and into the spherical harmonic representation in the MT spheres (9).

We calculate the Hartree potential in the G space as $V_H(\mathbf{G})=-4\pi n_+(\mathbf{G})/G^2$ [$n_+(\mathbf{G})$ is the positron density at the reciprocal lattice $\mathbf{G}$] and this potential is represented into the spherical harmonics in the MT spheres as Eq. (9) with

$$V_{lm}(r_0)=4\pi i^l \sum_{\mathbf{G}} V_H(\mathbf{G}) e^{i\mathbf{G}\mathbf{R}_\alpha} j_l(Gr_0) Y_{lm}^*(\hat{G}). \quad (23)$$

For the positron-electron correlation potential for the electrons (as well as the enhancement factor), similar to the correlation potential for the positron, we first calculate this potential in a real-space mesh based on the local electron and positron densities according to the TCDF theory within the LDA. This potential is transformed into the G space by the Fourier transform and finally is represented into the spherical harmonics in the MT spheres by using an expression similar to the above Eq. (23). After these implementations, the electron and positron wave functions are calculated iteratively until the self-consistency between the positron and electron densities is achieved. We have successfully applied this method to calculate the CDB spectra for the vacancy-oxygen aggregations in Si and the preliminary results were reported at the 12th international conference on positron annihilation.[58]

[1] *Positron Solid-State Physics*, edited by W. Brandt and A. Dupasquier (North-Holland, Amsterdam, 1995).
[2] K. G. Lynn, J. R. MacDonald, R. A. Boie, L. C. Feldman, J. D. Gabbe, M. F. Robbins, E. Bonderup, and J. Golovchenko, Phys. Rev. Lett. **38**, 241 (1977).
[3] K. G. Lynn, J. E. Dickman, W. L. Brown, M. F. Robbins, and E. Bonderup, Phys. Rev. B **20**, 3566 (1979).
[4] P. Asoka-Kumar, M. Alatalo, V. J. Ghosh, A. C. Kruseman, B. Nielsen, and K. G. Lynn, Phys. Rev. Lett. **77**, 2097 (1996).
[5] K. Saarinen, J. Nissilä, H. Kauppinen, M. Hakala, M. J. Puska, P. Hautojärvi, and C. Corbel, Phys. Rev. Lett. **82**, 1883 (1999).
[6] M. P. Petkov, M. H. Weber, K. G. Lynn, R. S. Crandall, and V. J. Ghosh, Phys. Rev. Lett. **82**, 3819 (1999).
[7] Y. Nagai, M. Hasegawa, Z. Tang, A. Hempel, K. Yubuta, T. Shimamura, Y. Kawazoe, A. Kawai, and F. Kano, Phys. Rev. B **61**, 6574 (2000).
[8] Y. Nagai, Z. Tang, M. Hasegawa, T. Kanai, and M. Saneyasu, Phys. Rev. B **63**, 134110 (2001).
[9] M. Alatalo, H. Kauppinen, K. Saarinen, M. J. Puska, H. Makinen, P. Hautojärvi, and R. M. Nieminen, Phys. Rev. B **51**, 4176 (1995).
[10] S. Szapala, P. Asoka-Kumar, B. Nielsen, J. P. Peng, S. Hayakawa, K. G. Lynn, and H.-J. Gossmann, Phys. Rev. B **54**, 4722 (1996).
[11] U. Myler, R. D. Goldberg, A. P. Knights, D. W. Lawther, and P. J. Simpson, Appl. Phys. Lett. **69**, 3333 (1996).
[12] J. Gebauer, M. Lausmann, T. E. M. Staab, R. Krause-Rehberg, M. Hakala, and M. J. Puska, Phys. Rev. B **60**, 1464 (1999).
[13] M. Alatalo, B. Barbiellini, M. Hakala, H. Kauppmen, T. Korhonen, M. J. Puska, K. Saarinen, P. Hautojärvi, and R. M. Nieminen, Phys. Rev. B **54**, 2397 (1996).
[14] J. Kuriplach, A. L. Morales, C. Dauwe, D. Segers, and M. Šob, Phys. Rev. B **58**, 10 475 (1998).
[15] V. J. Ghosh, B. Nielsen, and T. Friessnegg, Phys. Rev. B **61**, 207 (2000).
[16] V. J. Ghosh, M. Alatalo, P. Asoka-Kumar, B. Nielsen, K. G. Lynn, A. C. Kruseman, and P. E. Mijnarends, Phys. Rev. B **61**, 10 092 (2000).
[17] P. E. Mijnarends, A. C. Kruseman, A. van Veen, H. Schut, and A. Bansil, J. Phys.: Condens. Matter **10**, 10 383 (1998).
[18] E. Boroński and R. M. Nieminen, Phys. Rev. B **34**, 3820 (1986).
[19] M. J. Puska, A. P. Seitsonen, and R. M. Nieminen, Phys. Rev. B **52**, 10 947 (1995).
[20] M. J. Puska and R. M. Nieminen, Rev. Mod. Phys. **66**, 841 (1994).
[21] Z. Tang, M. Hasegawa, T. Chiba, M. Saito, H. Sumiya, Y. Kawazoe, and S. Yamaguchi, Phys. Rev. B **57**, 12 219 (1998).
[22] M. Saito and A. Oshiyama, Phys. Rev. B **53**, 7810 (1996).
[23] B. Barbiellini, M. J. Puska, T. Korhonen, A. Harju, T. Torsti, and R. M. Nieminen, Phys. Rev. B **53**, 16 201 (1996).
[24] D. M. Ceperley and B. J. Alder, Phys. Rev. Lett. **45**, 566 (1980).
[25] P. E. Mijnarends, in *Positron Solid-State Physics*, edited by W. Brandt and A. Dupasquier (North-Holland, Amsterdam, 1983), p. 146.
[26] P. E. Mijnarends and A. Bansil, in *Poistron Spectroscopy of Solids*, edited by A. Dupasquier and A. P. Mills, Jr. (IOS, Amsterdam, 1995), p. 25.
[27] J. Arponen and E. Pajanne, Ann. Phys. (N.Y.) **121**, 343 (1979).
[28] L. J. Lantto, Phys. Rev. B **36**, 5160 (1987).
[29] O. K. Anderson, Phys. Rev. B **12**, 3060 (1975).
[30] D. D. Koelling and G. O. Arbman, J. Phys. F: Met. Phys. **5**, 2041 (1975).
[31] D. S. Wang, A. J. Freeman, H. Krakauer, and M. Posternak, Phys. Rev. B **23**, 1685 (1981).
[32] H. J. F. Jansen and A. J. Freeman, Phys. Rev. B **30**, 561 (1984).
[33] L. F. Mattheiss and D. R. Hamann, Phys. Rev. B **33**, 823 (1986).
[34] P. Blaha and K. Schwarz, J. Phys. F: Met. Phys. **17**, 899 (1987).
[35] D. Singh, Phys. Rev. B **43**, 6388 (1991).
[36] D. J. Singh, *Planewaves, Pseudopotentials, and the LAPW Method* (Kluwer Academic, Boston, 1994).
[37] M. C. Payne, M. P. Teter, D. C. Allen, T. A. Arias, and J. D. Joannopoulos, Rev. Mod. Phys. **64**, 1045 (1992).
[38] R. Car and M. Parrinello, Phys. Rev. Lett. **55**, 2471 (1985).
[39] R. P. Gupta and R. W. Siegel, Phys. Rev. B **22**, 4572 (1980).
[40] S. Berko and J. S. Plaskett, Phys. Rev. **112**, 1877 (1958).
[41] D. J. Chadi and M. L. Cohen, Phys. Rev. B **8**, 5747 (1973).
[42] H. J. Monkhorst and J. D. Pack, Phys. Rev. B **13**, 5188 (1976).
[43] Y. Sakurai, Y. Tanaka, A. Bansil, S. Kaprzyk, A. T. Stewart, Y. Nagashima, T. Hyodo, S. Nanao, H. Kawata, and N. Shiotani, Phys. Rev. Lett. **74**, 2252 (1995).
[44] A. A. Manuel, D. Vasumathi, B. Barbiellini, A. Shukla, P. Suortti, and T. Chiba, Mater. Sci. Forum **255–257**, 760 (1997).
[45] S. Kahana, Phys. Rev. **129**, 1622 (1963).
[46] J. P. Carbotte and S. Kahana, Phys. Rev. **139**, A213 (1965).
[47] M. Šob, in *Proceedings of 8th Annual International Symposium on Electronic Structure of Metals and Alloys, Gaussig, Germany*, edited by P. Ziesche (Tech. Universität Dresden, 1978), p. 170.
[48] P. E. Mijnarends and R. M. Singru, Phys. Rev. B **19**, 6038 (1979).
[49] A. Rubaszek, Z. Szotec, and W. M. Temmerman, Phys. Rev. B **58**, 11 285 (1998).
[50] A. Rubaszek, Z. Szotec, and W. M. Temmerman, Phys. Rev. B **63**, 165 115 (2001).
[51] H.-E. Schaefer, R. Gugelmeier, M. Schmolz, and A. Seeger, Mater. Sci. Forum **15–18**, 111 (1987).
[52] T. Korhonen, M. J. Puska, and R. M. Nieminen, Phys. Rev. B **54**, 15 016 (1996).
[53] S. Berko, R. E. Kelley, and J. S. Plaskett, Phys. Rev. **106**, 824 (1957).
[54] Z. Tang, M. Hasegawa, T. Shimamura, Y. Nagai, T. Chiba, Y. Kawazoe, M. Takenaka, E. Kuramoto, and T. Iwata, Phys. Rev. Lett. **82**, 2532 (1999).
[55] M. Hasegawa, Z. Tang, Y. Nagai, T. Shimamura, K. Nakazuru, T. Chiba, and M. Saito, Mater. Sci. Forum **363–365**, 132 (2001).
[56] B. T. Kelly, *Physics of Graphite* (Applied Science, London, 1981).
[57] It should be noticed that the present case of graphite is somewhat special since the carbon atom has only a very small core so that the effect of using pseudo-wave-function is expected to be small.
[58] Z. Tang, T. Nonaka, Y. Nagai, and M. Hasegawa, Mater. Sci. Forum **363–365**, 67 (2001).